

# Pion distribution amplitude and form-factors: Improved Gaussian model of QCD vacuum

A. P. Bakulev<sup>1</sup>

*Joint Institute for Nuclear Research,  
Bogoliubov Lab. of Theoretical Physics,  
141980, Moscow Region, Dubna, Russia*

## Abstract

We describe the present status of the pion distribution amplitude (DA) as it originated from several sources: (i) a nonperturbative approach, based on QCD sum rules with nonlocal condensates, (ii) an  $O(\alpha_s)$  QCD analysis of the CLEO data on  $F^{\gamma\gamma^*\pi}(Q^2)$  with asymptotic and renormalon models for higher twists, and (iii) recent high-precision lattice QCD calculations of the second moment of the pion DA. Then we show the comparison of the results for the pion electromagnetic form factor, obtained in analytic perturbation theory, with JLab data on  $F_\pi(Q^2)$ . After that we introduce the improved model for nonlocal condensates in QCD and show its consequences for the pion DA and  $\gamma\gamma^* \rightarrow \pi$  transition form factor. In order to facilitate possible applications of BMS and improved “bunches” we suggest approximate analytic descriptions of their boundaries.

## 1 Generalized QCD SRs for mesonic distribution amplitudes

The pion distribution amplitude (DA) parameterizes the matrix element of the nonlocal axial current on the light cone [1]

$$\langle 0 | \bar{d}(z) \gamma_\mu \gamma_5 E(z, 0) u(0) | \pi(P) \rangle \Big|_{z^2=0} = i f_\pi P_\mu \int_0^1 dx e^{ix(zP)} \varphi_\pi^{\text{Tw-2}}(x, \mu^2). \quad (1)$$

The gauge-invariance of this DA is guarantied by the Fock–Schwinger string

$$E(z, 0) = \mathcal{P} \exp \left[ ig \int_0^z A_\mu(\tau) d\tau^\mu \right]$$

, inserted in between separated quark fields. Physical meaning of this DA is quite evident: it is the amplitude for the transition  $\pi(P) \rightarrow u(Px) + \bar{d}(P(1-x))$ . It is convenient to represent the pion DA using expansion in Gegenbauer polynomials  $C_n^{3/2}(2x-1)$ , which are one-loop eigenfunctions of ERBL kernel [2, 3]

$$\varphi_\pi(x; \mu^2) = \varphi^{\text{As}}(x) \left[ 1 + \sum_{n \geq 1} a_{2n}(\mu^2) C_{2n}^{3/2}(2x-1) \right], \quad (2)$$

where  $\varphi^{\text{As}}(x) = 6x(1-x)$  is the famous asymptotic DA. This representations means that all scale dependence in  $\varphi_\pi(x; \mu^2)$  is transformed to the scale dependence of the set

---

<sup>1</sup>E-mail: bakulev@theor.jinr.ru

$\{a_2(\mu^2), a_4(\mu^2), \dots\}$ . We mention here that ERBL solution at the 2-loop level is also possible with using the same representation (2) [4, 5, 6, 7].

In order to construct reliable QCD SRs for the pion DA moments one needs, as has been shown in [8, 9], to take into account the nonlocality of QCD vacuum condensates. For an illustration of the nonlocal condensate (NLC) model we use here the minimal Gaussian model

$$\langle \bar{q}(0)q(z) \rangle = \langle \bar{q}q \rangle e^{-|z^2|\lambda_q^2/8} \quad (3)$$

with a single scale parameter  $\lambda_q^2 = \langle k^2 \rangle$ , which characterizes the average momentum of quarks in the QCD vacuum. Its value has been estimated in QCD SR approach and also on the lattice[10, 11, 12, 13]:

$$\lambda_q^2 = 0.35 - 0.55 \text{ GeV}^2. \quad (4)$$

We see that  $\lambda_q^2$  is of an order of the typical hadronic scale  $m_\rho^2 \approx 0.6 \text{ GeV}^2$ .

Let us write down as an example the NLC QCD SR for the pion DA  $\varphi_\pi(x)$ . To produce it one starts with a correlator of currents  $J_{\mu 5}(x)$  and  $J_{\nu 5; N}^\dagger(0) = \bar{d}(0) \hat{n} \gamma_5 (n \nabla)^N u(0)$  with light-like vector  $n$ ,  $n^2 = 0$ , obtains SRs for the moments  $\langle x^N \rangle_\pi$  and then applies the inverse Mellin transform,  $\langle x^N \rangle_\pi \Rightarrow \varphi_\pi(x)$ . As a result we obtain

$$f_\pi^2 \varphi_\pi(x) = \int_0^{s_0} \rho^{\text{pert}}(x; s) e^{-s/M^2} ds + \frac{\alpha_s \langle GG \rangle}{24\pi M^2} \varphi_{GG}(x; \Delta) + \frac{8\pi\alpha_s \langle \bar{q}q \rangle^2}{81M^4} \sum_{i=2V, 3L, 4Q} \varphi_i(x; \Delta) \quad (5)$$

with  $\Delta \equiv \lambda_q^2/M^2$ . The local limit  $\Delta \rightarrow 0$  of this SR is specified by the appearance of  $\delta$ -functions concentrated at the end-points  $x = 0$  and  $x = 1$ , for example,  $\varphi_{4Q}(x; \Delta) = 9[\delta(x) + \delta(1-x)]$ .

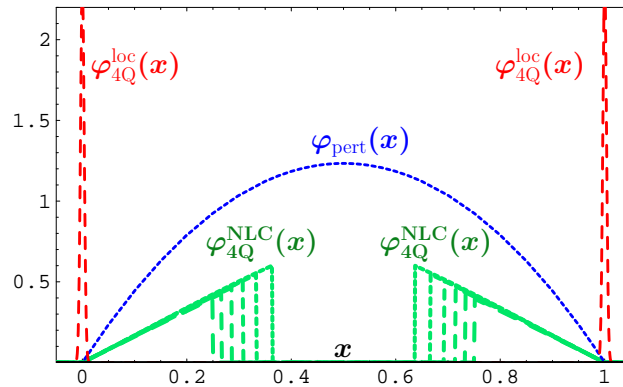


Figure 1: We show here contributions to the Eq. (5) due to perturbative loop (dotted line) and due to 4Q-condensate:  $\varphi_{4Q}^{\text{loc}}(x)$  — in standard QCD SRs, and  $\varphi_{4Q}^{\text{NLC}}(x, M^2 = 0.55 - 0.80 \text{ GeV}^2)$  — in NLC QCD SRs.

The minimal Gaussian model (3) generates the contribution  $\varphi_{4Q}(x; \Delta)$  shown in Fig. 1 in comparison with the perturbative one for the standard (local) and the NLC types of the SR. We see that due to completely different behaviour of perturbative and condensate terms in the local QCD SR case it is difficult to obtain some kind of consistency. Alternatively, the NLC contribution is much more similar to the perturbative one. Just by this reason we have very good stability in the NLC SR case! After processing SR (5) for the moments

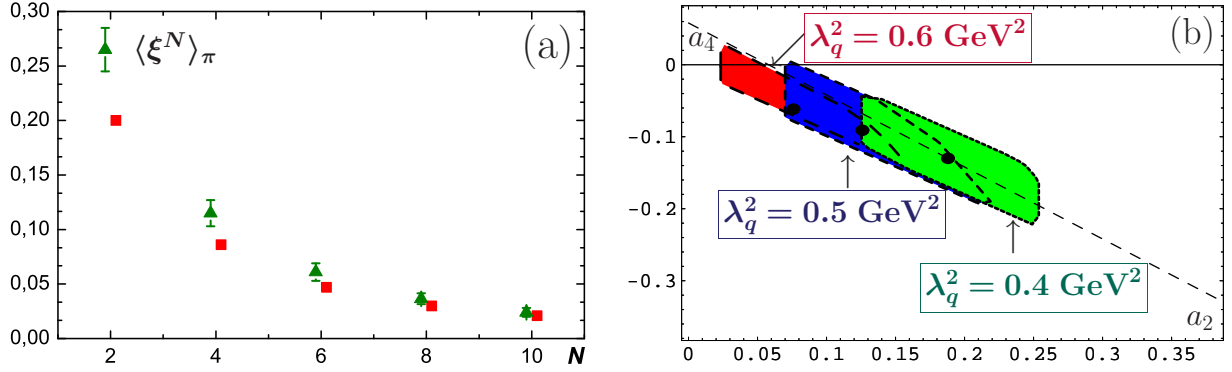


Figure 2: **Panel (a)**: Moments  $\langle \xi^N \rangle_\pi$  with  $N = 2, \dots, 10$ , obtained using the NLC SR (5), are shown by triangles with error-bars in comparison with the asymptotic DA moments (squares). **Panel (b)**: The allowed values of parameters  $a_2$  and  $a_4$  of the bunches (6), evaluated at  $\mu^2 = 1.35 \text{ GeV}^2$  for three values of the nonlocality parameter  $\lambda_q^2 = 0.4, 0.5$ , and  $0.6 \text{ GeV}^2$ .

$\langle \xi^N \rangle_\pi = \int_0^1 \varphi_\pi(x) (2x-1)^N dx$ , we restore the pion DA  $\varphi_\pi(x)$  by demanding that it should reproduce these first five moments  $\langle \xi^i \rangle_\pi$ ,  $i = 2, 4, \dots, 10$  with using the minimally possible number of the Gegenbauer harmonics in representation (2). It appears that NLC SRs for the pion DA produce a bunch of self-consistent 2-parameter models at  $\mu_0^2 \simeq 1.35 \text{ GeV}^2$ :

$$\varphi_\pi^{\text{NLC}}(x; \mu_0^2) = \varphi^{\text{As}}(x) \left[ 1 + a_2(\mu_0^2) C_2^{3/2}(2x-1) + a_4(\mu_0^2) C_4^{3/2}(2x-1) \right]. \quad (6)$$

The central point corresponds to  $a_2^{\text{BMS}} = +0.188$ ,  $a_4^{\text{BMS}} = -0.130$  in the case where  $\lambda_q^2 = 0.4 \text{ GeV}^2$ , whereas other allowed values of parameters  $a_2$  and  $a_4$  are shown in the left panel of Fig. 2 as the slanted rectangle [14]. By self-consistency of these solutions we understand that all of them produce, in accord with (6), the inverse moment of the pion DA

$$\langle x^{-1} \rangle_\pi^{\text{bunch}} = 3.17 \pm 0.20. \quad (7)$$

And this range is in a good agreement with the estimation dictated by the special SR for this moment, which can be obtained through the basic SR (5) by integration in  $x$  with the

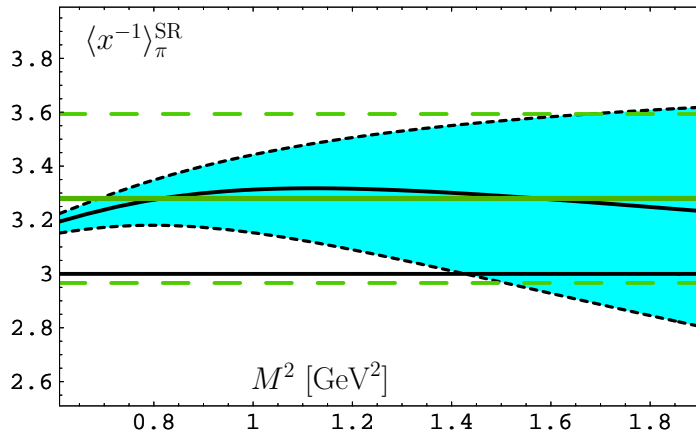


Figure 3: The inverse moment  $\langle x^{-1} \rangle_\pi$ , obtained using the NLC SR (5), is shown by the solid line (central value) with error-bars, shown as dashed lines.

corresponding weight  $x^{-1}$  (at  $\mu_0^2 \simeq 1.35 \text{ GeV}^2$ ):

$$\langle x^{-1} \rangle_\pi^{\text{SR}} = 3.30 \pm 0.30, \quad (8)$$

see Fig. 3. It is worth to emphasize here that the moment  $\langle x^{-1} \rangle_\pi^{\text{SR}}$  could be determined only in NLC SRs because there are no end-point singularities.

Comparing the obtained pion DA with the Chernyak&Zhitnitsky (CZ) one [15] reveals that although both DAs are two-humped they are quite different — BMS DA is strongly end-point suppressed, as illustrated in Fig. 4(a). To display this property more explicitly we show in the panel (b) of this figure the comparison of BMS and CZ contributions of different bins to inverse moment  $\langle x^{-1} \rangle_\pi$ , calculated as  $\int_x^{x+0.02} \varphi(x) dx$  and normalized to 100%.

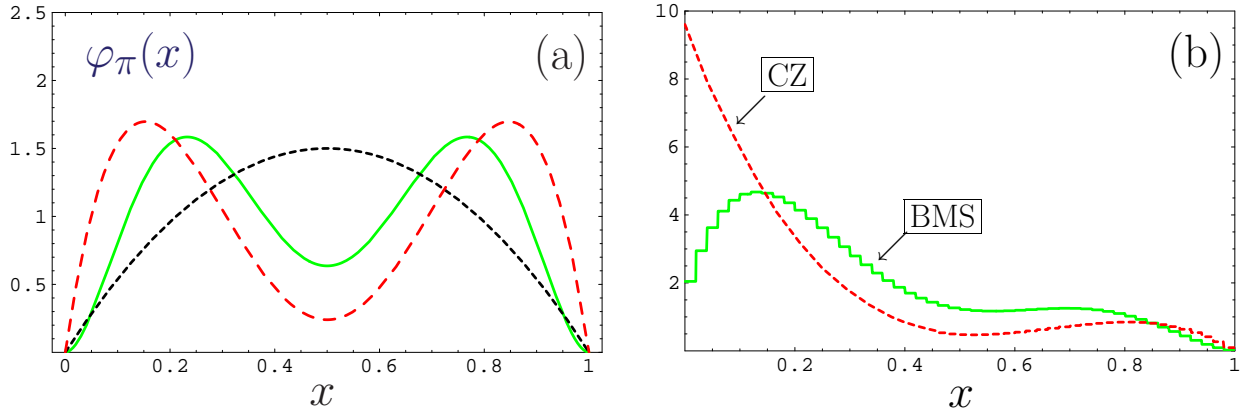


Figure 4: **Panel (a):** We compare here shapes of three DAs — BMS (solid line), CZ (dashed line), and the asymptotic DA (dotted line). **Panel (b):** Histograms for contributions of different bins to inverse moment  $\langle x^{-1} \rangle_\pi$  are shown for CZ and BMS DAs.

## 2 Analysis of CLEO data on $F_{\gamma\gamma^*\pi}(Q^2)$ and pion DA

Many studies [16, 17, 18, 13, 19, 20] have been performed in the literature to determine the pion DA using the high-precision CLEO data [21] on the pion-photon transition form factor  $F_{\pi\gamma^*\gamma}(Q^2)$ . In particular, in [19] we have used Light-Cone Sum Rules (LCSR) [22, 16] to the next-to-leading-order accuracy of QCD perturbation theory to examine the theoretical uncertainties involved in the CLEO-data analysis in order to extract more reliably the first two non-trivial Gegenbauer coefficients  $a_2$  and  $a_4$ , which parameterize the deviation from the asymptotic expression  $\varphi_\pi^{\text{As}}$ .

Why does one need to use Light-Cone SRs (LCSRs) in analyzing the experimental data on  $\gamma^*(Q)\gamma(q) \rightarrow \pi^0$ -transition form factor? For  $Q^2 \gg m_\rho^2$ ,  $q^2 \ll m_\rho^2$  the QCD factorization is valid only in the leading twist approximation and the higher twists are of importance [23]. The reason is quite clear: if  $q^2 \rightarrow 0$  one needs to take into account interaction of a real photon at long distances of order of  $O(1/\sqrt{q^2})$ . Then in order to account for long-distance effects in perturbative QCD one needs to introduce the light-cone DA of the real photon. Instead of doing so, Khodjamirian [22] suggested to use the LCSR approach, which effectively accounts for long-distances effects of the real photon using quark-hadron duality in the vector channel and dispersion relation in  $q^2$ . Schmedding and Yakovlev realized this approach to analyze the CLEO data on the  $\gamma^*\gamma \rightarrow \pi$  transition form factor with the next-to-leading-order (NLO) accuracy of perturbative QCD part of LCSR [16].

We improved the NLO analysis of the CLEO data by taking into account the following points: (i) the NLO evolution for both  $\varphi(x, Q_{\text{exp}}^2)$  and  $\alpha_s(Q_{\text{exp}}^2)$  with accurate taking into account heavy quark thresholds; (ii) the relation between the “nonlocality” scale and the twist-4 magnitude  $\delta_{\text{Tw-4}}^2 \approx \lambda_q^2/2$  was used to re-estimate  $\delta_{\text{Tw-4}}^2 = 0.19 \pm 0.02$  at  $\lambda_q^2 = 0.4 \text{ GeV}^2$ ; (iii) the possibility to extract constraints on  $\langle x^{-1} \rangle_\pi$  from the CLEO data and to compare them with those we have from NLC QCD SRs.

Results of our analysis [19] are displayed in Fig. 5. Solid lines in all figures enclose the  $2\sigma$ -contours, whereas the  $1\sigma$ -contours are enclosed by dashed lines. The three slanted and shaded rectangles represent the constraints on  $(a_2, a_4)$  posed by the QCD SRs [14] for corresponding values of  $\lambda_q^2 = 0.6, 0.5, 0.4 \text{ GeV}^2$  (from left to right). All values are evaluated at  $\mu^2 = 2.4 \text{ GeV}^2$  after the NLO evolution.

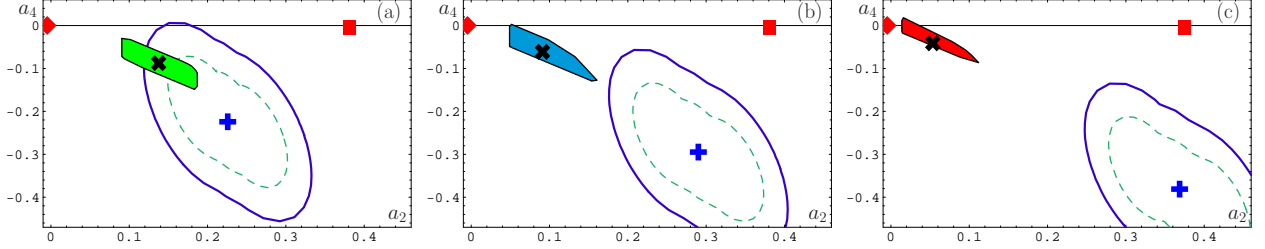


Figure 5: Three  $2\sigma$ - and  $1\sigma$ -contours (solid and dashed lines, correspondingly) of the admissible regions following from the analysis of the CLEO data for different values of  $\delta^2$ : (a) – for  $\lambda_q^2 = 0.4 \text{ GeV}^2$  and  $\delta^2 = (0.19 \pm 0.02) \text{ GeV}^2$ ; (b) – for  $\lambda_q^2 = 0.5 \text{ GeV}^2$  and  $\delta^2 = (0.235 \pm 0.025) \text{ GeV}^2$ ; (c) – for  $\lambda_q^2 = 0.6 \text{ GeV}^2$  and  $\delta^2 = (0.29 \pm 0.03) \text{ GeV}^2$ .

We see that the CLEO data definitely prefer the value of the QCD nonlocality parameter  $\lambda_q^2 = 0.4 \text{ GeV}^2$ . We also see in Fig. 5(c) (and this conclusion was confirmed even with 20% uncertainty in twist-4 magnitude, see also Fig. 6(a)) that CZ DA (■) is excluded at least at  $4\sigma$ -level, whereas the asymptotic DA (◆) — at  $3\sigma$ -level. In the same time our DA (X) and most of the bunch (the slanted green-shaded rectangle around the symbol X) are inside  $1\sigma$ -domain. Instanton-based Bochum (☆) and Dubna (▲) models are near  $3\sigma$ -boundary and only the Krakow model [24], denoted in Fig. 6(a) by symbol ◆, is close to  $2\sigma$ -boundary.

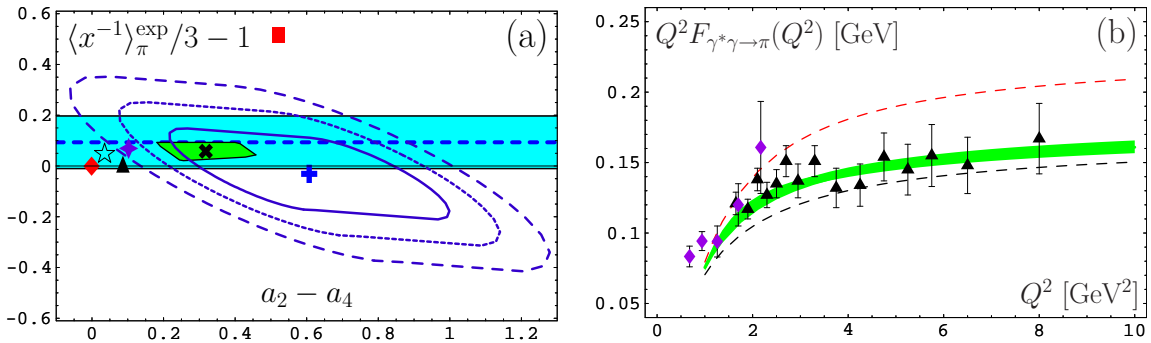


Figure 6: (a): The results of the CLEO data analysis for the pion DA parameters ( $\langle x^{-1} \rangle_\pi^{\text{exp}}/3 - 1$ , evaluated at  $\mu_0^2 \approx 1 \text{ GeV}^2$ ). (b): LCSR predictions for  $Q^2 F_{\gamma^* \gamma \rightarrow \pi}(Q^2)$  for the CZ DA (upper dashed line), BMS-“bunch” (shaded strip), and the asymptotic DA (lower dashed line) in comparison with the CELLO (diamonds, [25]) and the CLEO (triangles, [21]) experimental data, evaluated with the twist-4 parameter value  $\delta_{\text{Tw-4}}^2 = 0.19 \text{ GeV}^2$  [19] and at  $\mu_{\text{SY}}^2 = 5.76 \text{ GeV}^2$ .

In Fig. 6(a) we demonstrate the  $1\sigma$ -,  $2\sigma$ - and  $3\sigma$ -contours (solid, dotted and dashed contours around the best-fit point ( $\blacklozenge$ )), which have been obtained for values of the twist-4 scale parameter  $\delta_{\text{Tw-4}}^2 = [0.15 - 0.23] \text{ GeV}^2$ . As one sees from the blue dashed line within the hatched band, corresponding in this figure to the mean value of  $\langle x^{-1} \rangle_\pi^{\text{SR}}/3 - 1$  and its error bars, the nonlocal QCD sum-rules result with its error bars appears to be in good agreement with the CLEO-constraints on  $\langle x^{-1} \rangle_\pi^{\text{exp}}$  at the  $1\sigma$ -level. Moreover, the estimate  $\langle x^{-1} \rangle_\pi^{\text{SR}}$  is close to  $\langle x^{-1} \rangle_\pi^{\text{EM}}/3 - 1 = 0.24 \pm 0.16$ , obtained in the data analysis of the electromagnetic pion form factor within the framework of a different LCSR method in [26, 27]. These three independent estimates are in good agreement to each other, giving firm support that the CLEO data processing, on one hand, and the theoretical calculations, on the other, are mutually consistent.

Another possibility, suggested in [28], to obtain constraints on the pion DA in the LCSR analysis of the CLEO data – to use for the twist-4 contribution renormalon-based model, relating it then to parameters  $a_2$  and  $a_4$  of the pion DA. Using this method we obtain [29] the renormalon-based constraints for the parameters  $a_2$  and  $a_4$ , shown Fig. 8 in the form of  $1\sigma$ -ellipse (dashed contour).

### 3 Dijet E791 data, pion form factor and CEBAF data

Our findings are further confirmed by the E791 data [30] on diffractive dijet  $\pi + A$ -production. This is illustrated in Fig. 7(a). The main conclusion here is that all considered pion DAs are consistent with the data, with tiny preference to the BMS DA. Indeed, following the convolution procedure of [31] we found [19] the following values of  $\chi^2$  for three types of pion DAs: 12.56 (asymptotic DA), 10.96 (BMS bunch), and 14.15 (CZ DA).

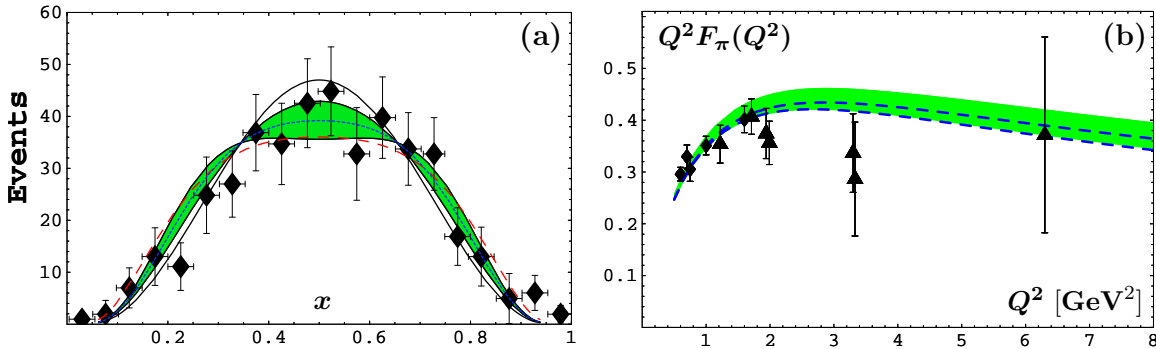


Figure 7: **(a)**: Comparison with the E791 data on diffractive dijet production of the BMS “bunch” (shaded strip), the asymptotic DA (solid line), and the CZ (dashed line) model, using the convolution approach of [31]. **(b)**: The scaled pion form factor calculated with the BMS bunch (shaded strip) and asymptotic DA (dashed lines) including nonperturbative uncertainties from NLC QCD SRs [14] and renormalization scheme and scale ambiguities at the  $O(\alpha_s^2)$ -level [32]. The experimental data are taken from [33] (diamonds) and [34], [35] (triangles).

It is worth to mention here also the results of our analysis of the pion electromagnetic form factor using NLC dictated pion DA and Analytic Perturbative QCD [32]. These results are in excellent agreement with CEBAF data on pion form factor, as illustrated in the Fig. 7(b), where the green strip includes both the NLC QCD SRs uncertainties, generated by our bunch of the allowed pion DA, and by the scale-setting ambiguities at the NLO level.

From the phenomenological point of view, the most interesting result here is that the BMS pion DA [14] (out of a “bunch” of similar doubly-peaked endpoint-suppressed pion DAs) yields to predictions for the electromagnetic form factor very close to those obtained with the asymptotic pion DA. Conversely, we see that a small deviation of the prediction for the pion form factor from that obtained with the asymptotic pion DA does not necessarily imply that the underlying pion DA has to be close to the asymptotic profile. Much more important is the behavior of the pion DA in the endpoint region  $x \rightarrow 0, 1$ .

## 4 New lattice data and pion DA

Rather recently new high-precision lattice measurements of the pion DA second moment  $\langle \xi^2 \rangle_\pi = \int_0^1 (2x - 1)^2 \varphi_\pi(x) dx$  appeared [36, 37]. Both groups extracted from their respective simulations, values of  $a_2$  at the Schmedding–Yakovlev scale  $\mu_{\text{SY}}^2$  around 0.24, but with different error bars.

It is remarkable that these lattice results are in striking agreement with the estimates of  $a_2$  both from NLC QCD SRs [14] and also from the CLEO-data analyses—based on LCSR—[16, 19], as illustrated in Fig. 8(a), where the lattice results of [37] are shown in the form of a vertical strip, containing the central value with associated errors. Noteworthily, the value of  $a_2$  of the displayed lattice measurements (middle line of the strip) is very close to the CLEO best fit in [19] (+).

## 5 Improved model for NLCs and pion DA

The quark-gluon-antiquark condensates are usually parameterized in the following form

$$\begin{aligned} \langle \bar{q}(0) \gamma_\mu (-g \hat{A}_\nu(y)) q(x) \rangle &= (y_\mu x_\nu - g_{\mu\nu}(yx)) \overline{M}_1(x^2, y^2, (y-x)^2) \\ &+ (y_\mu y_\nu - g_{\mu\nu} y^2) \overline{M}_2(x^2, y^2, (y-x)^2), \\ \langle \bar{q}(0) \gamma_5 \gamma_\mu (-g \hat{A}_\nu(y)) q(x) \rangle &= i \varepsilon_{\mu\nu\gamma x} \overline{M}_3(x^2, y^2, (y-x)^2), \end{aligned}$$

with  $(A_{1,2,3} = A_0(-\frac{3}{2}, 2, \frac{3}{2}))$

$$\overline{M}_i(x^2, y^2, z^2) = A_i \iiint_0^\infty d\alpha d\beta d\gamma f_i(\alpha, \beta, \gamma) e^{(\alpha x^2 + \beta y^2 + \gamma z^2)/4}. \quad (9)$$

The minimal model of nonlocal QCD vacuum suggests the following Ansatz

$$f_i(\alpha, \beta, \gamma) = \delta(\alpha - \Lambda) \delta(\beta - \Lambda) \delta(\gamma - \Lambda) \quad (10)$$

with  $\Lambda = \frac{1}{2} \lambda_q^2$  and faces problems with QCD equations of motion and gauge invariance of 2-point correlator of vector currents. In order to fulfil QCD equations of motion exactly and minimize non-transversity of  $V - V$  correlator we suggest [38] the improved model of QCD vacuum with

$$f_i^{\text{imp}}(\alpha, \beta, \gamma) = (1 + X_i \partial_x + Y_i \partial_y + Z_i \partial_z) \delta(\alpha - x\Lambda) \delta(\beta - y\Lambda) \delta(\gamma - z\Lambda), \quad (11)$$

where  $z = y$ ,  $\Lambda = \frac{1}{2} \lambda_q^2$  and

$$X_1 = +0.082; X_2 = -1.298; X_3 = +1.775; x = 0.788; \quad (12a)$$

$$Y_1 = -2.243; Y_2 = -0.239; Y_3 = -3.166; y = 0.212. \quad (12b)$$

Then the NLC sum rules 5 produce [38] a “*bunch*” of 2-parameter pion DA models (6) at  $\mu^2 = 1.35 \text{ GeV}^2$ . The coordinates of the central point  $\blacklozenge$  are  $a_2 = 0.268$  and  $a_4 = -0.186$ . These values correspond to  $\langle x^{-1} \rangle_\pi^{\text{bunch}} = 3.24 \pm 0.20$ , which is in agreement with the result of an independent sum rule, viz.,  $\langle x^{-1} \rangle_\pi^{\text{SR}} = 3.40 \pm 0.34$ . In order to facilitate possible applications of our “bunches” we suggest the following approximate analytic descriptions of their boundaries — we specify upper and lower curves,  $a_4^\pm(a_2)$ , and left and right vertical lines, fixed by their abscissa values,  $a_2^{\text{L,R}}$ :

$$a_4^{\text{BMS},+}(a_2) = 0.177 - 2.41 a_2 + 7.77 a_2^2 - 14.0 a_2^3; \quad (13a)$$

$$a_4^{\text{BMS},-}(a_2) = -0.027 - 0.246 a_2 - 4.12 a_2^2 + 8.86 a_2^3; \quad (13b)$$

$$a_2^{\text{BMS},\text{L}} = 0.134; \quad a_2^{\text{BMS},\text{R}} = 0.251, \quad (13c)$$

for the BMS bunch, whereas for the improved bunch

$$a_4^{\text{BP},+}(a_2) = 0.352 - 4.25 a_2 + 14.0 a_2^2 - 18.9 a_2^3; \quad (14a)$$

$$a_4^{\text{BP},-}(a_2) = 0.588 - 6.89 a_2 + 20.7 a_2^2 - 23.6 a_2^3; \quad (14b)$$

$$a_2^{\text{BP},\text{L}} = 0.177; \quad a_2^{\text{BP},\text{R}} = 0.346. \quad (14c)$$

Allowed values of both bunch parameters  $a_2$  and  $a_4$  after NLO-evolution to  $\mu^2 = 5.76 \text{ GeV}^2$  are shown in Fig. 8 in a form of shaded slanted rectangles around central points  $\blacktimes$  and  $\blacklozenge$ .

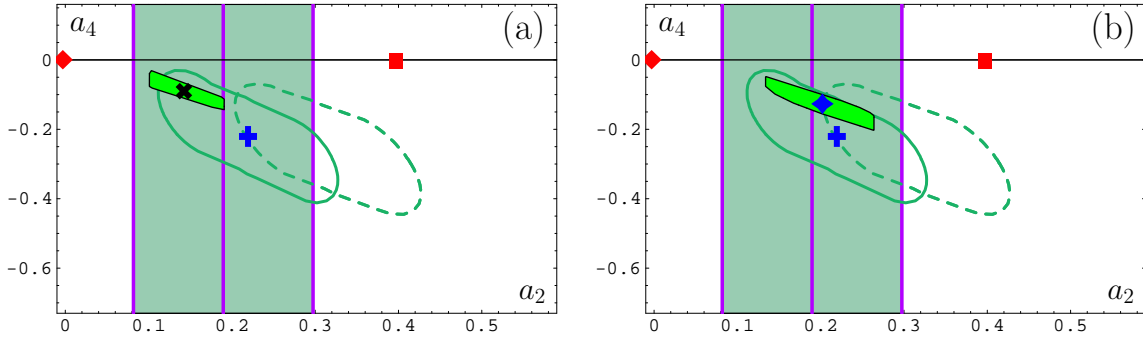


Figure 8: The results of the CLEO data analysis for the pion DA parameters  $a_2$  and  $a_4$ , evaluated at  $\mu_{\text{SY}}^2 = 5.76 \text{ GeV}^2$ . The lattice results of [37] are shown for comparison as shaded area, whereas the renormalon-based  $1\sigma$ -ellipse of [29] is displayed by the green dashed line. The shaded strip in panel (a) shows the corresponding results for the BMS-“bunch”, whereas in panel (b) — the new bunch, corresponding to the improved Gaussian model of QCD vacuum.

We emphasize here that BMS model [14], shown in Fig. 8(a) by symbol  $\blacktimes$ , is inside the allowed region dictated by the improved QCD vacuum model. This means that all the characteristic features of the BMS bunch are also valid for the improved bunch: NLC-dictated models are end-point suppressed, although are double-humped.

We see in Fig. 8(b) that the improved bunch [38] is even in a better agreement with the recent lattice results [37], shown in the form of a vertical strip, containing the central value with associated errors. Remarkably, the value of  $a_2$  of the displayed lattice measurements (middle line of the strip) is very close to the central point of the “improved bunch” ( $\blacklozenge$ ), whereas the whole bunch, dictated by the improved NLC QCD SRs [38], is inside the strip<sup>2</sup> and completely inside the standard CLEO  $1\sigma$ -ellipse.

<sup>2</sup>The same is valid for the BMS “bunch” as well, as can be seen in Fig. 8(a).

## 6 Conclusions

Let me conclude with the following observations:

- NLC QCD SR method for the pion DA gives us the admissible bunches of DAs for each value of  $\lambda_q$ .
- NLO LCSR method produces new constraints on the pion DA parameters ( $a_2$  and  $a_4$ ) in conjunction with the CLEO data.
- Comparing results of the NLC SRs with new CLEO constraints allows to fix the value of QCD vacuum nonlocality:  $\lambda_q^2 = 0.4 \text{ GeV}^2$ .
- This bunch of pion DAs agrees well E791 data on diffractive dijet  $\pi + A$ -production, with JLab F(pi) data on the pion form factor, and with recent lattice data.
- Taking into account QCD equations of motion for NLCs and transversity of vacuum polarization allows us to put the pion DA bunch just inside  $1\sigma$ -ellipse of CLEO-data constraints.

## Acknowledgments

This investigation was supported in part by the Heisenberg–Landau Programme, grant 2006, and the Russian Foundation for Fundamental Research, grants No. 06-02-16215.

## References

- [1] A. V. Radyushkin, Dubna preprint P2-10717, 1977 [hep-ph/0410276].
- [2] A.V. Efremov and A.V. Radyushkin, Phys. Lett. 94B (1980) 245; Teor. Mat. Fiz. 42 (1980) 147 [Theor. Math. Phys. 42 (1980) 97].
- [3] G.P. Lepage and S.J. Brodsky, Phys. Lett. 87B (1979) 359; Phys. Rev. D22 (1980) 2157.
- [4] S. V. Mikhailov and A. V. Radyushkin, Nucl. Phys. **B273**, 297 (1986).
- [5] E. P. Kadantseva, S. V. Mikhailov, and A. V. Radyushkin, Sov. J. Nucl. Phys. **44**, 326 (1986).
- [6] D. Müller, Phys. Rev. **D49**, 2525 (1994); *ibid.* **D51**, 3855 (1995).
- [7] A. P. Bakulev and N. G. Stefanis, Nucl. Phys. **B721**, 50 (2005).
- [8] S. V. Mikhailov and A. V. Radyushkin, JETP Lett. **43**, 712 (1986); Sov. J. Nucl. Phys. **49**, 494 (1989); Phys. Rev. **D45**, 1754 (1992).
- [9] A. P. Bakulev and S. V. Mikhailov, Phys. Lett. **B436**, 351 (1998).
- [10] V. M. Belyaev and B. L. Ioffe, ZhETF **83**, 876 (1982).
- [11] A. A. Ovchinnikov and A. A. Pivovarov, Sov. J. Nucl. Phys. **48**, 721 (1988).

- [12] M. D’Elia, A. Di Giacomo, and E. Meggiolaro, Phys. Rev. **D59**, 054503 (1999).
- [13] A. P. Bakulev and S. V. Mikhailov, Phys. Rev. **D65**, 114511 (2002).
- [14] A. P. Bakulev, S. V. Mikhailov, and N. G. Stefanis, Phys. Lett. **B508**, 279 (2001); in *Proceedings of the 36th Rencontres De Moriond On QCD And Hadronic Interactions, 17–24 Mar 2001, Les Arcs, France*, edited by J. T. T. Van (World Scientific, Singapore, 2002), pp. 133–136.
- [15] V. L. Chernyak and A. R. Zhitnitsky, Nucl. Phys. **B201**, 492 (1982); *ibid.* **B214**, 547(E) (1983).
- [16] A. Schmedding and O. Yakovlev, Phys. Rev. **D62**, 116002 (2000).
- [17] N. G. Stefanis, W. Schroers, and H.-C. Kim, Phys. Lett. **B449**, 299 (1999); Eur. Phys. J. **C18**, 137 (2000).
- [18] E. Ruiz Arriola and W. Broniowski, Phys. Rev. **D66**, 094016 (2002).
- [19] A. P. Bakulev, S. V. Mikhailov, and N. G. Stefanis, Phys. Rev. **D67**, 074012 (2003); Phys. Lett. **B578**, 91 (2004).
- [20] S. S. Agaev, Phys. Rev. D **72**, 114010 (2005).
- [21] J. Gronberg *et al.*, Phys. Rev. **D57**, 33 (1998).
- [22] A. Khodjamirian, Eur. Phys. J. **C6**, 477 (1999).
- [23] A. V. Radyushkin and R. Ruskov, Nucl. Phys. **B481**, 625 (1996).
- [24] M. Praszalowicz and A. Rostworowski, Phys. Rev. **D64**, 074003 (2001).
- [25] H. J. Behrend *et al.*, Z. Phys. **C49**, 401 (1991).
- [26] V. M. Braun, A. Khodjamirian, and M. Maul, Phys. Rev. **D61**, 073004 (2000).
- [27] J. Bijnens and A. Khodjamirian, Eur. Phys. J. **C26**, 67 (2002).
- [28] S. S. Agaev, Phys. Rev. **D72**, 114010 (2005).
- [29] A. P. Bakulev, S. V. Mikhailov, and N. G. Stefanis, Phys. Rev. **D73**, 056002 (2006).
- [30] E. M. Aitala *et al.* (Fermilab E791), Phys. Rev. Lett. **86**, 4768 (2001).
- [31] V. M. Braun *et al.*, Nucl. Phys. **B638**, 111 (2002).
- [32] A. P. Bakulev *et al.*, Phys. Rev. **D70**, 033014 (2004).
- [33] J. Volmer *et al.*, Phys. Rev. Lett. **86**, 1713 (2001).
- [34] C. N. Brown *et al.*, Phys. Rev. **D8**, 92 (1973).
- [35] C. J. Bebek *et al.*, Phys. Rev. **D13**, 25 (1976).
- [36] L. Del Debbio, Few Body Syst. **36**, 77 (2005).
- [37] V. M. Braun *et al.*, Phys. Rev. **D74**, 074501 (2006).
- [38] A. P. Bakulev and A. V. Pimikov, hep-ph/0608288.